Journal of Non-Crystalline Solids 573 (2021) 121134

Contents lists available at ScienceDirect

Journal of Non-Crystalline Solids

journal homepage: www.elsevier.com/locate/jnoncrysol

Features in low-temperature electrical resistivity of amorphous Cd_3As_2 films due to hopping conductivity with changing activation energy

E.A. Piluyk [a], O.N. Ivanov [a,b,*], V.S. Zakhvalinskii [a], T.B. Nikulicheva [a,c]

[a] Belgorod State University, Belgorod 308015, Russian Federation
[b] Belgorod State Technological University named after V.G. Shukhov, Belgorod 308012, Russian Federation
[c] LLC "Fund for Innovative Science-Intensive Technologies", Belgorod 308518, Russian Federation

ARTICLE INFO

Keywords:
Cd_3As_2
Amorphous films
Negative magnetoresistance
Activation energy
Variable-range hopping conductivity

ABSTRACT

Amorphous Cd_3As_2 films were deposited on single-crystalline $SrTiO_3$ substrate by high-frequency non-reactive magnetron sputtering. Electrical resistivity of the film, measured within 3-75 K range, increases at cooling. Below ~70 K, negative transverse magnetoresistance observed. Features in electrical resistivity and magnertoresistance can be attributed to variable-range hopping conductivity of the Mott type with local activation energy, which is temperature-dependent. Two temperature ranges in the hopping conductivity observed. Appearing two ranges is in qualitative accordance with the Mott-Davis energy-band model developed for amorphous semiconductors. High temperature range of the hopping conductivity is attributed to electron hops between localized states, positioned inside band tails, whereas electron hops between localized states, positioned inside Fermi-peak, can be responsible for low-temperature range. At taking into account temperature dependences of local activation energy, universal expression for various mechanisms of the hopping conductivity could be successfully applied to analyze the experimental data.

1. Introduction

It is known that hopping conductivity of various types is often dominant mechanism of low-temperature electrical conductivity of disordered (amorphous) and heavily doped semiconductors [1–13]. The hopping conductivity is due to tunneling hops of electron from one localized state to another one. For heavily doped semiconductors, the localized states are positioned inside an impurity band, which can be partially overlapped with conductivity or valence band [2]. In amorphous semiconductors the localized states correspond to relatively narrow peak of the density of states, which is positioned at the Fermi level near mid of energy gap [1]. This Fermi-peak is originated from a structural disorder due to different defects like dangling bonds, vacancies, etc. Besides this narrow peak, conductivity and valence band tails with the localized states are also characteristic features of amorphous semiconductors. The tails are originated from destroying long-range order and they can be overlapped or not overlapped with the Fermi-peak. At high enough temperatures, a thermal generation of electrons into the localized states of the band tails or the Fermi-peak can take place that will result in the hopping conductivity. There are several mechanisms of the hopping conductivity including variable-range hopping (VRH) conductivity and nearest-neighbor hopping (NNH) conductivity. Each of the mechanisms can be described by relevant temperature law [1,2]. For amorphous semiconductors, the VRH conductivity of the Mott type is usually observed [1], whereas the VRH conductivity of the Efros-Shklovskii type is more typical for heavily doped semiconductors [2]. The differences for these types of the hopping conductivity are strongly originated from specific features in energy band structure of amorphous and heavily doped semiconductors. Generally, many of the conductivity mechanisms, responsible for temperature behavior of the electric properties of solids within relevant temperature range, are thermally activated processes with activation energy, E_a, which is T-independent for this temperature range. In this case, temperature dependence of the conductivity can be reliably and informatively analyzed. The VRH conductivity is also thermally activated process, but E_a is usually T-dependent. The $E_a(T)$ variation complicates analyzing temperature behavior of the conductivity. Instead of T-independent E_a, local activation energy, E_{al}, taking into account T-variation of E_a, should be introduced [2].

In this paper, we report specific features in the low-temperature electrical resistivity of amorphous Cd_3As_2 films, which can be analyzed in frames of the VRH conductivity of the Mott type with T-

* Corresponding author at: Belgorod State Technological University named after V.G. Shukhov, Belgorod 308012, Russian Federation.
E-mail address: olniv@mail.ru (O.N. Ivanov).

https://doi.org/10.1016/j.jnoncrysol.2021.121134
Received 27 April 2021; Received in revised form 11 August 2021; Accepted 19 August 2021
Available online 27 August 2021

dependent activation energy.

2. Materials and methods

Thin Cd_3As_2 films were grown by high-frequency non-reactive magnetron sputtering with a nominal radiation power of 10 W in Ar atmosphere with a residual pressure of 0.8 Pa. Single-crystalline $SrTiO_3$ was applied as a substrate. Substrate temperature during the deposition process was equal to 293 K. Sputtering target was prepared from pre-synthesized Cd_3As_2 single crystals with sizes of several mm each. To synthesize the single crystals, the Cd (99.999%) and As (99.99%) powders, taken in stoichiometric ratio, were directly melted together.

To confirm amorphous state of the film grown, X-ray diffraction (XRD) analysis was performed by using a Rigaku Ultima IV diffractometer with CuK_α–radiation. To estimate Cd-to-As ratio in the film, energy dispersive X-ray spectroscopy (EDX) method was applied by using a Nova NanoSEM 450 microscope. Scanning electron microscopy (SEM) performing the same microscope was also applied to estimate thickness of the film. To analyze chemical and phase composition of the film, Raman scattering spectra were recordered by using a LabRam HR Evolution Raman spectrometer, which applies a laser with a wavelength of 532 nm, a power of 50 mW, and a spectral resolution of 0.5 cm^{-1}.

A Mini Cryogen Free Measurements System (Cryogenic Ltd, UK) was applied to measure the specific electrical resistivity and examine the Hall effect. To take temperature and magnetic field dependences of ρ, a film 5 × 2 mm sample with thickness of d was prepared. Four-probe method was used. Gold contacts were deposited onto the sample by magnetron sputtering. Magnetic field, B= 5 T, was applied perpendicularly to current direction flowing in sample plane that corresponds to transverse magnetoresistance. Density of measuring current was equal to 1 $A{\cdot}cm^{-2}$. The ρ measurements were carried out by reversing measuring current. The accuracy of the ρ measurements was equal to 3 %.

3. Results and discussion

3.1. Characterization of the films

Primarily, it is important to note that XRD pattern, taken from the film being studied at room temperature, is characterized by appearance of a “halo” pattern (Fig. 1). Generally, the “halo” is characteristic of amorphous state [14,15]. So, the film should be considered as an “X-ray amorphous” material. In according with EDX data, the Cd-to-As ratio in the film is equal to ~1.53 that is in well accordance with its stoichiometric composition. However, a small Cd excess can result in relevant forming As vacancies, which are the source of unintentional n-type doping in the film being studied, since in accordance with the Hall effect examination, the majority carriers in the film are electrons [16]. For further analyzing the film, the Raman spectroscopy method was applied. Raman spectrum of the film is presented in Fig. 2 (curve *1*). As a reference, the Raman spectrum for the Cd_3As_2 single crystal, used as a target for film sputtering, is presented, too (curve *2*). It is known that two main Raman peaks, centered around 200 (P_1) and 250 cm^{-1} (P_2), are characteristic of Cd_3As_2 [17,18]. These peaks are observed for both the single crystal and the film. However, for the single-crystalline Cd_3As_2 the peaks are rather sharp, narrow and intense, whereas in the amorphous film they are broader and less intense. Besides, a broad Raman peak (band), centered at ~290 cm^{-1} (P_3), is additionally appeared in the spectrum of the film

In comparison with crystalline solid, amorphous Cd_3As_2 film is less orderly in its arrangement with a wider array of bond angles, bond energies and bond lengths existing in addition to dangling bonds. The distribution of possible states can result in the broad P_3 band that is readily distinguishable from that of crystalline solid. In general, the difference between curves *1* and *2* in Fig. 2 is typical feature for the crystalline and amorphous states of solid and it can be usually attributed to a partial destroying of long-range order in the amorphous state [19]. Therefore, one can conclude that the film being studied is the amorphous Cd_3As_2 one.

To estimate the film thickness, d, cross-sectional SEM image of the “Cd_3As_2 film” – “$SrTiO_3$ substrate” system was taken and analyzed (Fig. 3). The film is well d-homogeneous with d≈50 nm.

3.2. Features in the low-temperature electrical resistivity

The $\rho(T)$ dependence for the film being studied taken at zero magnetic field within the 3-75 K range is presented in Fig. 4 (a). The resistivity is steady increasing with decreasing temperature that corresponds to a semiconductor behavior. An unusual magnetic field effect on ρ was found. At low temperatures this effect is negative, since ρ decreases under 5 T magnetic field. In contrast to this behavior, at high temperatures ρ already increases at applying B, but this positive B-effect on ρ is very weak, since the $\rho(T)$ curves, taken for zero and 5 T magnetic fields, are positioned very close to each other. Inset to Fig. 4 (a) shows the $\rho(T)$ dependences for B=0 (curve *1*) and 5 T (*2*) corresponding to the negative B-effect. The $MR(T)$ dependence, calculated for these magnetic

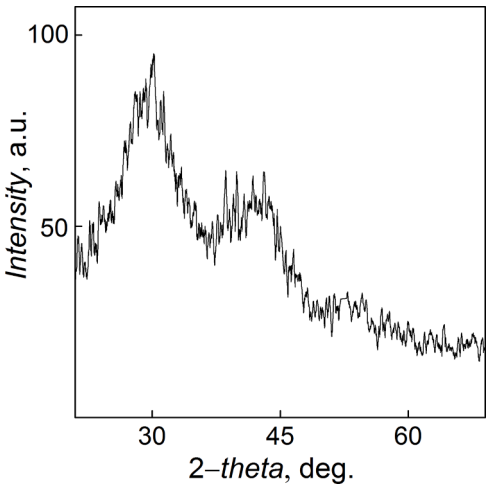

Fig. 1. XRD pattern of the film.

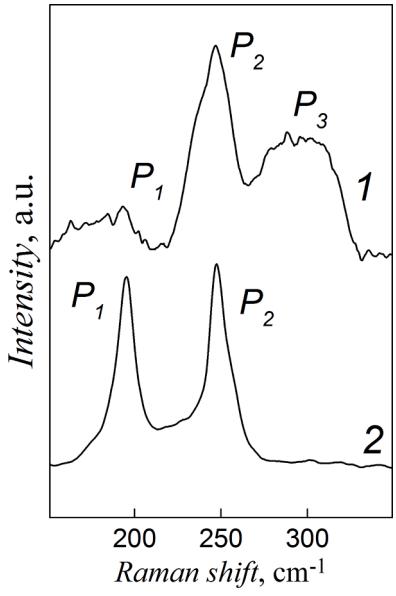

Fig. 2. Raman spectra for the amorphous Cd_3As_2 film (curve *1*) and the Cd_3As_2 single crystal.

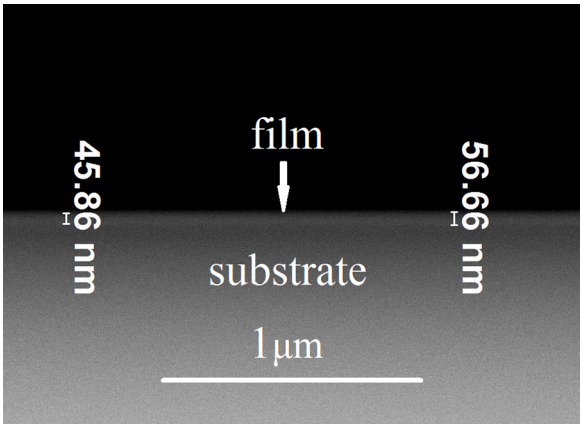

Fig. 3. Cross-sectional SEM image of the film-substrate system.

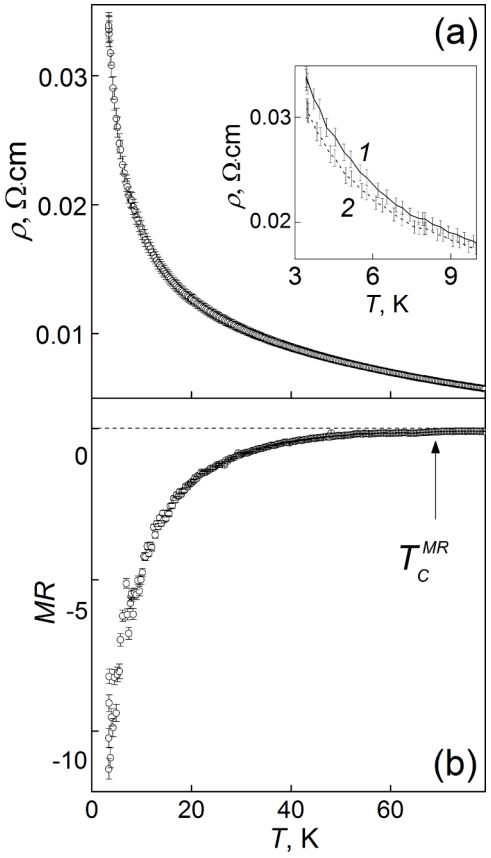

Fig. 4. (a) The $\rho(T)$ dependence taken at zero magnetic field. Insets: large-scale part of the $\rho(T)$ dependences taken at for B=0 (curve *1*) and 5 T (*2*); (b) The *MR* (*T*) dependence calculated for B=0 and 5 T. Below T_C^{MR} negative magnetoresistance starts to develop.

fields as [($\rho(T, B$=5 T)-($\rho(T, B$=0 T)]/$\rho(T, B$=0 T), is presented in Fig. 4 (b). This dependence summarizes all the features in the *B*-effect on ρ listed above. Thus, one can conclude that at $T_C^{MR} \approx 70\ K$ a crossover from the positive *B*-effect on ρ to the negative one takes place. Besides, the negative *B*-effect is much stronger expressed as compared to the positive *B*-effect, and magnitude of the negative *B*-effect is rapidly increasing with decreasing temperature. The T_C^{MR} temperature is also related to change in the conductivity mechanism of the film, and the lower temperature mechanism is characterized by the negative *MR*. Magnetoresistance in solids is commonly observed as positive one, which is associated with cyclotron motion of carriers under external magnetic field. The negative *MR* can be originated from several special cases. For instance, the negative *MR* is usually observed in a ferromagnet, in which the polarization of electrons and their scattering can be affected by a magnetic field [20–23]. A weak localization of electrons in two-dimensional systems which falls off in the presence of a magnetic field can also result in a negative *MR* in a low field [24–28]. Besides, the negative *MR* can be also considered as specific sign of the variable-range hopping conductivity [28–32].

Generally, the $\rho(T)$ behavior related to the thermally activated conductivity obeys a law as follows [33]

$$\rho(T) \sim exp\left(\frac{E_a}{k_B T}\right)^p, \tag{1}$$

where k_B is the Boltzmann constant and p is the exponent depending on conductivity mechanism.

In accordance with expression (1) and provided the E_a energy is *T*-independent, E_a can be estimated from a slope of linear segments in the lnρ vs. $(1/T)$ dependence, which can be calculated from initial experimental $\rho(T)$ curve. Usually, each of the linear segments, characterizing by its *T*-independent E_a, corresponds to relevant conductivity mechanism. The ln$\rho(1/T)$ dependence, calculated from the $\rho(T)$ dependence presented in Fig. 4 (a), is shown in Fig. 5 (a). For the temperature range used, no linear segments observed in this dependence. Therefore, the activation energy cannot be considered as *T*-independent, and, as was

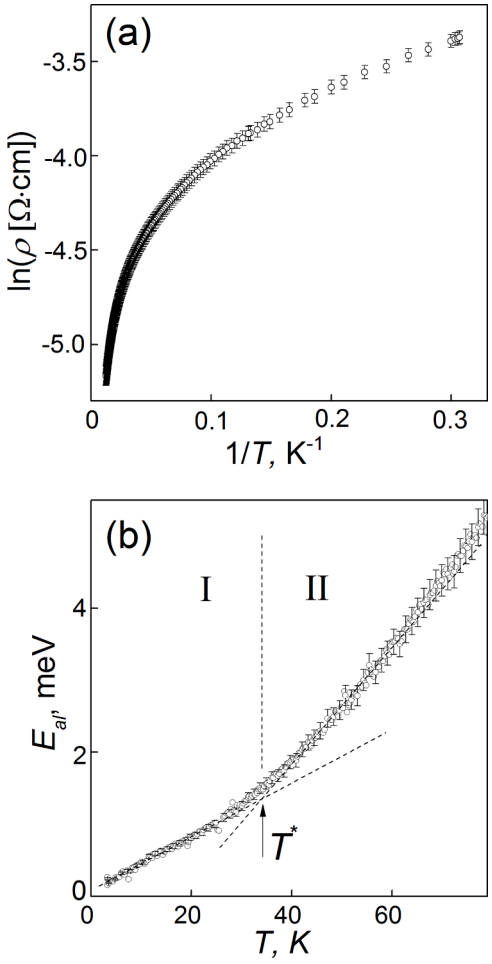

Fig. 5. The ln(ρ) vs. $1/T$ (a) and the E_{al} vs. T (b) dependences taken at zero magnetic field. The E_{al} vs. T dependence consists of two linear segments crossing at T^* as shown by dashed lines. The lines are drawn as guides to the eyes.

mentioned above, the local T-dependent activation energy should be involved to describe the $\rho(T)$ dependence in this case. The local activation energy can be found as [2,4]

$$E_{al} = \frac{d(ln\rho)}{d\left(\frac{1}{k_B T}\right)}. \quad (2)$$

The $E_{al}(T)$ dependence consists of two linear segments, I and II, differing its slopes (Fig. 5 (b)). These I and II segments, corresponding to low-temperature and high-temperature range of the electrical conductivity, intersect at temperature $T^*\approx 33$ K. Both $E_{al}(T)$ segments can be described by equation of a straight line

$$E_{al}(T) = C + K \cdot T, \quad (3)$$

where C and K are fitting constants (C is the E_{al} value, where the straight line cuts the y-axis, and K is angular coefficient).

The fitting constants were extracted as $K^I = 4 \cdot 10^{-2}$ meV·K^{-1} and $C^I = 0$ meV (for the I segment), and $C^{II} = -3.16$ meV and $K^{II} = 9.5 \cdot 10^{-2}$ meV·K^{-1} (for the II segment). Different mechanisms of the hopping conductivity with T-dependent activation energy occuring in disordered and heavily doped semiconductors can be described by the following universal expression [4]

$$\rho(T) = A \cdot T^q \cdot exp\left(\frac{E_{al}}{k_B \cdot T}\right)^m, \quad (4)$$

where A is the constant, m and q are the exponents depending on regime of the hopping conductivity.

Taking into account Eq. (3) and values of the fitting constants, expression (4) can be rewritten as

For the low-temperature rangr (I):

$$\rho^I(T) = A \cdot T^q \cdot exp\left(\frac{K^I \cdot T}{k_B T}\right)^m = A^I \cdot T^q \quad (5.1)$$

For the high-temperature range (II):

$$\rho^{II}(T) = A \cdot T^q \cdot exp\left(\frac{C^{II} + K^{II} \cdot T}{k_B T}\right)^m = A^{II} \cdot T^q \cdot exp\left(\frac{C^{II}}{k_B \cdot T}\right)^m, \quad (5.2)$$

where A^I and A^{II} are new fitting constants for the I and II segments, respectively. These constants do not contribute into the temperature behaviour of the specific electrical resistivity. So, exact expression for these constants are not under discussion here.

Therefore, the $\rho^I(T)$ dependence for the I segment happens to be governed by only pre-exponential T-dependent power factor with the q exponent, whereas the $\rho^{II}(T)$ dependence for the II segment is originated from, firstly, the same pre-exponential power factor and, secondly, exponential factor with the m exponent. It was found that the best fitting the experimental $\rho(T)$ curve corresponds to $q = -3/4$ for the I segment (Fig. 6 (a)), and $m = 1/4$ and $q = -3/4$ for the II segment. Actually, the ρ vs. $T^{-3/4}$ dependence is linear at $T < T^*$ (Fig. 6 (a)), whereas the $\ln(\rho \cdot T^{-3/4})$ vs. $T^{-1/4}$ dependence is linear at $T > T^*$ (Fig. 6 (b)).

Therefore, taking into account the fitting T-linear $E_{al}(T)$ expressions, extracted for high temperature and low-temperature ranges, universal expression for various mechanisms of the hopping conductivity was successfully applied to very well describe the experimental $\rho(T)$ curve. The $m = 1/2$ value is characteristic of the VRH conductivity of the Mott type, and $q = -3/4$ value is related to wave function of the localized states expressed as [5]

$$\psi(r) \sim r^{-1} exp\left(-\frac{r}{a}\right), \quad (6)$$

where a is the localization radius of electron and r is the radius-vector.

Two temperature ranges in the VRH conductivity observed (Fig. 6 (a) and (b)) can be associated with two types of energy bands containing the localized states. In accordance with the Mott-Davis energy-band model

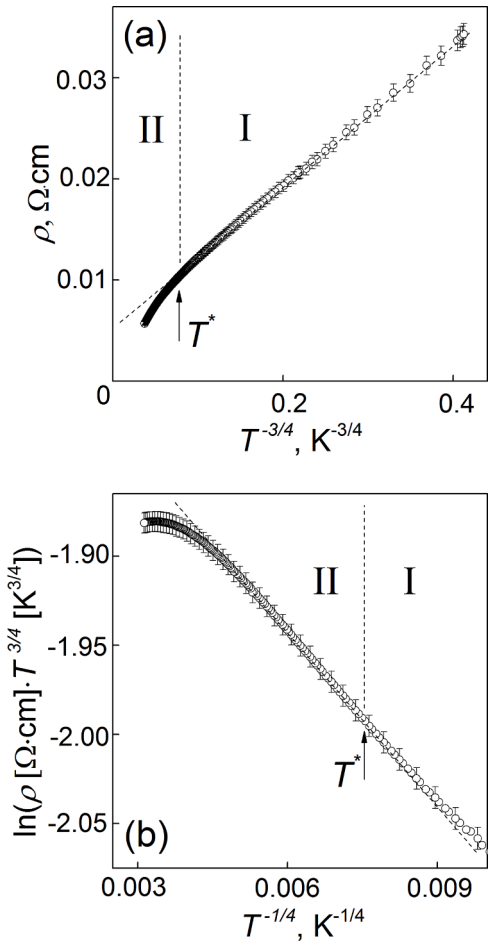

Fig. 6. The ρ vs. $T^{-3/4}$ (a) and $\ln(\rho \cdot T^{-3/4})$ vs. $T^{-1/4}$ (b) dependences taken at zero magnetic field. The I and II fields correspond to two regimes of variable-range hopping conductivity differing in fitting constant. The fitting lines are shown by dashed lines. The lines are drawn as guides to the eyes.

[1], these bands are characteristic of amorphous semiconductors. Specific features of amorphous semiconductor are, firstly, destroying a long-range atomic order and, secondly, forming numerous defects like dangling bonds, vacancies, etc. Owing to the first feature resulting in local varying the atom-atom distance and bond energy, the edges of conductivity and valence bands of amorphous semiconductor becomes indistinct, diffusing into the band gap. As result, the band tails, positioned inside the energy gap, formed. Due to the second feature, a narrow peak in the density of defect states is formed in mid of thee energy gap near the Fermi level, E_F (so called Fermi-peak). Energy band diagram corresponding to the Mott-Davis model is schematically shown in Fig. 7 (a). In this diagram, the density of states, $N(E)$, at $E > E_C$ (for electrons) and at $E < E_V$ (for holes) corresponds to extended states like states in the allowed bands with the Bloch states of a crystalline material. The density of states continues through the E_C and E_V points, which limit the band gap in a crystalline material, but the electrical conductivity below E_C (for electrons) and above E_V (for holes) is abruptly changed from conductivity through the extended states to the conductivity through the localized states (*LST*) for electrons immediately below E_C (holes immediately above E_V). The density of the localized states remains very high throughout the energy gap. Other localized sates are positioned inside the Fermi-peak (*LSFP*). Therefore, two types of the localized states, related to the band tails or the Fermi-peak, exist in amorphous semiconductor. Depending on temperature, the VRH conductivity could be observed for one or other types of these localized states. To initiate the hopping conductivity, electron should get ability to

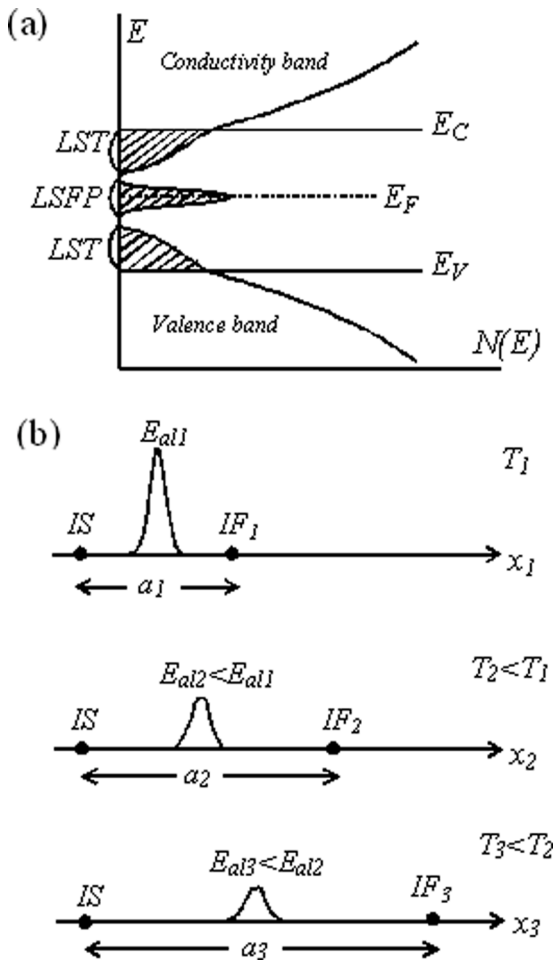

Fig. 7. (a) Energy band diagram of amorphous semiconductor showing the localized states positioned inside the conductivity and valence band tails (*LST*) and inside the Fermi-peak (*LSFP*); (b) Schematic of the VRH conductivity showing a link between the electron hop distance and the local activation energy (*IS* is the initial localized state, which is the same for all the temperatures, IF_i (i=1,2 and 3) is the final localized state).

hop via tunneling from one initial localized state into a final localized state. The hopping conductivity is a thermally activated process characterizing by the activation energy. At the nearest-neighbor hopping conductivity, the electron, localized in the initial state, hops to the final localized state, which is nearest one. The initial and final localized states are close in space but far in energy. With decreasing temperature, a probability of electron hops between the nearest-neighbor localized states gradually decreases, but the hopping distance is strongly T-independent.

The VRH conductivity will take place, if this probability will happen to be smaller as compared to that for electron hopping between some more spatially remote states, but whose energy levels are positioned close enough to each other. As result, with decreasing temperature for the VRH conductivity, the activation energy should be decreasing and with simultaneous increasing in the average hopping distance, a, since electron in the initial localized state (*IS*) will always find more remote but more energetically benefit final localized state (*IF*). Schematic of the VRH conductivity showing a link between the electron hop distance and the local activation energy is shown in Fig. 7 (b). As for our experiment, the high-temperature VRH conductivity (at $T>T^*$) should be reasonably related to the band-tail localized states, then the low-temperature VRH conductivity (at $T<T^*$) would be naturally originated from the Fermi-peak localized states.

The activation energy of the VRH conductivity of the Mott type can be expressed by the characteristic temperature, T_0, as follows [2]

$$E_a = \frac{T_0}{k_B} = \frac{\beta_m}{k_B k g(E_F)\alpha^3}, \tag{7}$$

where k is the dielectric permittivity, $g(E_F)$ is the density of states at the Fermi level, and β_m is the constant equal to 21.

For the amorphous Cd_3As_2 film being studied, the activation energy happened to be T-dependent local activation energy. Suppose, that expression (7) can be also applied to definite the local activation energy. According to this expression, the $E_{al}(T)$ dependence can be attributed to relevant $g(E_F)$ dependence. Both E_a and E_{al} are finding via derivative of $d(\ln\rho)/d(1/T)$, and E_a is T-independent, but E_{al} is T-dependent. To come to the T-linear E_{al} dependence observed in our experiment (Fig. 5 (b)), one should suppose that the $g(E_F)$ is T-dependent (the $g(E_F)\sim 1/T$ condition should be valid). In turn, the temperature dependence on $g(E_F)$ can be related to a temperature drift of E_F. To explain the T-linear E_{al} dependence, this $E_F(T)$ drift and exact $N(E)$ dependences corresponding to both the band tails and the Fermi-peak should be correctly taken into account. At present, getting these data is rather complicated task.

The negative magnetic field effect on ρ, observed within temperature ranges of the VRH conductivity (Fig. 4 (b)), can be reasonably attributed to increasing in the localization radius of electron. The radius is known to be B-dependent parameter [2]. With increasing magnetic field α can be either increasing or decreasing value. Decreasing in α, resulting in the negative magnetoresistance, is originated from damping of a quantum interference of hopping electrons in external magnetic field. Increasing in α, resulting in the positive magnetoresistance, is due to shrinkage of the electron wave functions in the direction perpendicular to B. Since the magnetoresistance of the amorphous Cd_3As_2 films is negative, the damping of the quantum interference can be taken as main mechanism responsible for the B-effect on ρ in this case. According to the Hall effect examination, the majority carriers in the film being studied are electrons. Within whole temperature range under study, the electron concentration happened to be T-independent end equal to $\sim 2\cdot 10^{18}$ cm^{-3}. Temperature dependence of the Hall mobility of electrons, μ_H, is shown in Fig. 8. At $T>T^*$, μ_H steady decreases with decreasing temperature. However, below T^*, μ_H starts to abruptly decrease. The abrupt decreasing in the carrier mobility, known as forming a mobility gap, is usually observed at transition from conductivity through the extended states to the conductivity through the localized states. In our experiments, such kind of the gap is obviously formed at transition from the high-temperature VRH conductivity to the low-temperature VRH

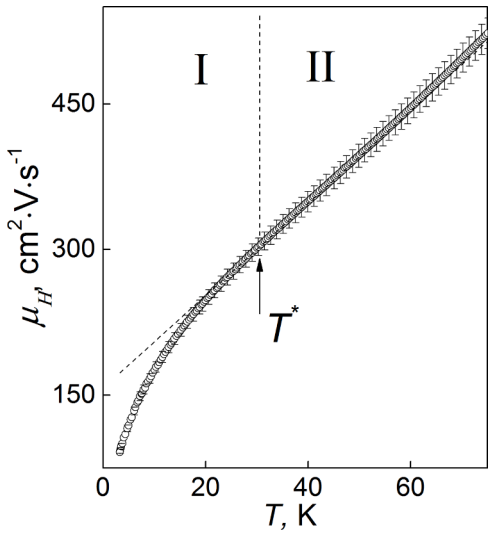

Fig. 8. The $\mu_H(T)$ dependence taken at zero magnetic field. Below T^* the electron mobility starts to abruptly decrease. The line is drawn as guides to the eyes to indicate T^*.

conductivity. Again, specific features of energy band diagram should be correctly taken into account to explain the $\mu_H(T)$ behavior.

Conclusion

High-frequency non-reactive magnetron sputtering has been applied to deposit the amorphous Cd_3As_2 films on single-crystalline $SrTiO_3$ substrate. Features in the low-temperature electrical properties of the films are characteristic of the variable-range hopping conductivity of the Mott type with T-dependent local activation energy. These features including the negative magnetoresistance and the semiconducting $\rho(T)$ behavior are in qualitative agreement with the Mott-Davis energy-band model developed for amorphous semiconductors.

CRediT authorship contribution statement

E.A. Piluyk: Project administration. **O.N. Ivanov:** Writing – review & editing. **V.S. Zakhvalinskii:** Investigation. **T.B. Nikulicheva:** Investigation.

Declaration of Competing Interest

The authors declare that they have no known competing financial interests or personal relationships that could have appeared to influence the work reported in this paper.

Acknowledgments

The work was also financially supported by the Russian Science Foundation under grant No 19-79-00152. All of studies were carried out by the scientific equipment of joint research center "Technologies and Materials" at the Belgorod State University.

References

[1] N.F. Mott, E.A. Davis, Electronic Processes in Non-crystalline Materials, Oxford University Press, 1979.
[2] L. Efros, B.I. Shklovskii, Electronic Properties of Doped Semiconductor, Springer, Berlin, 1984.
[3] G.K. van Ancum, M.A.J. Verhoeven, D.H.A. Blank, H. Rogalla, Electric-field activated variable-range hopping transport in $PrBa_2Cu_{307-\delta}$, Phys. Rev. B. 52 (1995) 5598, https://doi.org/10.1103/PhysRevB.52.5598.
[4] R. Laiho, A.V. Lashkul, K.G. Lisunov, E. Lahderanta, M.A. Shakhov, V. S. Zakhvalinskii, Hopping conductivity of Ni-doped p-CdSb, J. Phys. Condens. Mater. 20 (2008), https://doi.org/10.1088/0953-8984/20/29/295204, 295204-1-8.
[5] R. Laiho, K.G. Lisunov, E. Lahderanta, P.A. Petrenko, J. Salminen, M.A. Shakhov, M.O. Safontchik, V.S. Stamov, M.V. Shybnikov, V.S. Zakhvalinskii, Variable-range hopping conductivity in $La_{1-x}Ca_xMn_{1-y}Fe_yO_3$: evidence of a complex gap in density of states near the Fermi level, J. Phys. Condens. Mater. 14 (2002) 8043–8055, https://doi.org/10.1088/0953-8984/14/34/323.
[6] Y. Yao, B. Bo, C. Liu, The hopping variable range conduction in amorphous in as thin films, Curr. Appl. Phys. 18 (2018) 1492–1495, https://doi.org/10.1016/j.cap.2018.09.005.
[7] A.I. Kolyubakin, V.E. Antonov, O.I. Barkalov, A.F. Gurov, A.I. Harkunov, Transport properties od bulk amorphous $Al_{32}Ge_{68}$, J. Non-Cryst. Solids 289 (2001) 30–36, https://doi.org/10.1016/S0022-3093(01)00645-7.
[8] A. Yildiz, N. Serin, T. Serin, M. Kasap, Crossover from nearest-neighbor hopping conduction to Efros–Shklovskii variable-range hopping conduction in hydrogenated amorphous silicon films, Jpn. J. Appl. Phys. 48 (2009), https://doi.org/10.1143/JJAP.48.111203, 111203-1-5.
[9] M. Fujii, Y. Inoue, S. Hayashi, K. Yamamoto, Hopping conduction in SiO_2 films containing C, Si, and Ge clusters, Appl. Phys. Lett. 68 (1996) 3749–3751, https://doi.org/10.1063/1.115994.
[10] J. Han, M. Shen, W. Cao, A.M.R. Senos, P.Q. Mantas, Hopping conduction in Mn-doped ZnO, Appl. Phys. Lett. 82 (2003) 67–69, https://doi.org/10.1063/1.1535262.
[11] E. Arushanov, S. Siebentritt, T. Schedel-Niedrig, M. Ch, Lux-Steiner, Hopping conductivity in p-$CuGaSe_2$ films, J. Appl. Phys. 100 (2006), https://doi.org/10.1063/1.2338600, 063715-1-4.
[12] O. Ivanov, M. Yaprintsev, Variable-range hopping conductivity in Lu-doped Bi_2Te_3, Solid State Sci. 76 (2018) 111–117, https://doi.org/10.1016/j.solidstatesciences.2017.12.012.
[13] O. Ivanov, M. Yaprintsev, E. Danshina, Electric field effect on variable-range hopping conductivity in $Bi_{1.9}Lu_{0.1}Te_3$, Phys. B Condens. Matter 545 (2018) 222–227, https://doi.org/10.1016/j.physb.2018.06.021.
[14] Z.H. Stachurski, On structure and properties of amorphous materials, Mater 4 (2011) 1564–1598, 10.3390.ma4091564.
[15] R.K. Biswas, P. Khan, S. Mukherjee, A.K. Mukhopadhyay, J. Ghosh, K. Muraleedharan, Study of short range structure of amorphous Silica from PDF using Ag radiation in laboratory XRD system, RAMAN and NEXAFS, J. Non-Cryst. Solids 488 (2018) 1–9, https://doi.org/10.1016/j.jnoncrysol.2018.02.037.
[16] T. Schumann, M. Goyal, D.A. Kealhofer, S. Stemmer, Negative magnetoresistance due to conductivity fluctuations in films of the topological semimetal Cd_3As_2, Phys. Rev. B. 95 (2017), https://doi.org/10.1103/PhysRevB.95.241113, 241113-1-6.
[17] S. Wei, J. Lu, W. Yu, H. Zhang, Y. Qian, Isostructural Cd_3E_2 (E=P, As) microcrystals prepared via a hydrothermal route, Cryst. Growth Des. 849 (2006) 849–853, https://doi.org/10.1021/cg049589u.
[18] P. Cheng, C. Zhang, Y. Liu, X. Yuan, F. Song, Q. Sun, P. Zhou, D.W. Zhang, F. Xiu, Thickness-dependent quantum oscillations in Cd_3As_2 thin films, New J. Phys. 18 (2016), https://doi.org/10.1088/1367-2630/18/8/083003, 083003-1-9.
[19] J.H. Dias da Silva, S.W. da Silva, J.C. Galzerani, Crystallization process of amorphous GaSb films studied by Raman spectroscopy, J. Appl. Phys. 77 (1995) 4044–4048, https://doi.org/10.1063/1.359486.
[20] A.B. Pippard, Magnetoresistance in Metals, Cambridge University, Cambridge, 1989.
[21] L. Xing, X. Gui, W. Xie, H. Cao, J. Yan, B.C. Sales, R. Jin, Mn-induced ferromagnetic semiconducting behavior with linear negative magnetoresistance in $Sr_4(Ru_{1-x}Mn_x)_3O_{10}$ single crystals, Sci. Rep. 8 (2018), https://doi.org/10.1038/s41598-018-31679-w, 1330-1-8.
[22] I. Tsukada, T. Yamamoto, M. Takagi, T. Tsubone, S. Konno, K. Uchinokura, Ferromagnetism and large negative magnetoresistance in Pb doped Bi–Sr–Co–O misfit-layer compound, J. Phys. Soc. Jpn. 70 (2001) 834–840, https://doi.org/10.1143/JPSJ.70.834.
[23] Z.W. Fan, P. Li, H.L. Ba, Large negative magnetoresistance and ferromagnetism induceby interfacial spins in granular Cr/C films, JMMM 368 (2014) 267–272, https://doi.org/10.1016/j.immm.2014.05.046.
[24] L. Kilanski, R. Szymczak, W. Dobrowolski, A. Podgórni, A. Avdonin, V.E. Slynko, E. I. Slynko, Negative magnetoresistance and anomalous hall effect in GeMnTe-SnMnTe spin-glass-like system, J. Appl. Phys. 113 (2013), https://doi.org/10.1063/1.4790321, 063702-1-4.
[25] H. Xue, Y. Hong, C. Li, J. Meng, Y. Li, K. Liu, M. Liu, W. Jiang, Z. Zhang, L. He, R. Dou, C. Xiong, J. Nie, arge negative magnetoresistance driven by enhanced weak localization and Kondo effect at the interface of $LaAlO_3$ and Fe-doped $SrTiO_3$, Phys. Rev. B 98 (2018), https://doi.org/10.1103/PhysRevB.98.08530, 085305-1-7.
[26] Y. Wang, J.J. Santiago-Avilés, Large negative magnetoresistance and two-dimensional weak localization in carbon nanofiber fabricated using electrospinning, J. Appl. Phys. 94 (2003), https://doi.org/10.1063/1.1587268, 1721-1-5.
[27] W.E. Liu, E.M. Hankiewicz, D. Culcer, Weak localization and antilocalization in topological materials with impurity spin-orbit interactions, Materials 10 (2017), https://doi.org/10.3390/ma10070807, 807-1-21.
[28] H. Mell, J. Stuke, Negative magnetoresistance of amorphous semiconductors, J. Non-Cryst. Solids 4 (1970) 304–310, https://doi.org/10.1016/0022-3093(70)90055-4.
[29] K.G. Lisunov, E. Arushanov, Variable-range hopping conductivity and magnetoresistance in n-$CuGaSe_2$, J. Appl. Phys. 88 (2000), https://doi.org/10.1063/1.1290454, 4128-1-7.
[30] H.L. Zhao, B.Z. Spivak, M.P. Gelfand, S. Feng, Negative magnetoresistance in variable-range-hopping conduction, Phys. Rev. B. Condens. Matter. 44 (1991) 10760–10767, https://doi.org/10.1103/PhysRevB.44.10760.
[31] A. Sybous, Negative magnetoresistance behaviour and variable range hopping conduction in insulating NbSi amorphous alloys at very low temperature with magnetic field, J. Mod. Phys. 3 (2012) 521–528, https://doi.org/10.4236/jmp.2012.37071.
[32] K.H. Kim, S. Lara-Avila, H. He, H. Kang, S.J. Hong, M. Park, J. Eklöf, K. Moth-Poulsen, S. Matsushita, K. Akagi, S. Kubatkin, Y.W. Park, Probing variable range hopping lengths by magneto conductance in carbonized polymer nanofibers, Sci. Rep. 8 (2018), https://doi.org/10.1038/s41598-018-23254-0, 4948-1-8.
[33] J.S. Blakemore, Solid State Physics, Cambridge University Press, Cambridge, 1985.